DOI: 10.1002/
Article type: Full Paper

Nanocrystal Inks: Photoelectrochemical Printing of Cu_2O Nanocrystals on Silicon with Two-Dimensional Control on Polyhedral Shapes

Yan B. Vogel, Vinicius R. Gonçales, Louai Al-Obaidi, J. Justin Gooding, Nadim Darwish* and Simone Ciampi**

Y. B. Vogel, L. Al-Obaidi, Dr. N. Darwish, Dr. S. Ciampi
Curtin Institute of Functional Molecules and Interfaces
Curtin University
Bentley, Western Australia 6102, Australia
E-mail: simone.ciampi@curtin.edu.au, nadim.darwish@curtin.edu.au

Dr. V. R. Gonçales, Prof. J. J. Gooding
School of Chemistry
The University of New South Wales
Kensington, New South Wales 2052, Australia
E-mail: Justin.gooding@unsw.edu.au

Keywords: silicon functionalization, cuprous oxide nanoparticle patterns, crystal shapes, nanoparticle gradients, photoelectrochemistry

Abstract text. Here is reported a printing technology that enables the functionalization of photoconducting materials with an arbitrary user-defined pattern of nanocrystals. Two sets of information can be encoded into the same unit area; control over the polyhedral shape of individual nanocrystals and high lateral resolution (micrometre scale) for large 2D patterns (millimetre scale) of Cu_2O that were grown over unstructured amorphous silicon. Key to this new technology is a parallel modulation of both the electrode kinetics at the silicon/electrolyte interface as well as the light-assisted control of adsorption of halide ions on the growing Cu_2O particles. This is achieved using local pixelation of a visible light stimuli by means of adapting to the field of photoelectrochemistry the instrumental tools for spatial light modulation more often used in super resolution microscopy. Any user-defined pattern (*i.e.*, any arbitrary bitmap image file or a sequence of images) is converted within seconds into an array of nanoparticles. The process does not rely on the use of physical masks

or chemical templating and it is parallel, meaning for example that it is possible to guide the exclusive growth of cubic nanoparticles in an area defined at will by the operator, while the neighbouring section(s) are being covered exclusively by octahedrons.

1. Introduction

Evidence of attempts to protect brands and revenues traces back to ancient China, with the first use of trademarks identifying manufacturers dating back to 3000 B.C..[1] Counterfeited goods and documents is now a trillion dollar global problem.[2] Conventional track-and-trace technologies such as RFID chips are of great value, both in terms of authentication as well as deterrence. Less visible "track" only security products, such as DNA tags (*e.g.*, SafeTraces),[3] something akin to a molecular barcode, are becoming available but will probably be limited to the food or bio-security markets.[4] Any advance in traditional anti-counterfeiting platforms, such as in image printing[5] and colour-shifting inks,[6] or in rapidly evolving technologies such as holograms,[7] will inevitably become available to the same party who aims to replicate such a form of security pattern.[8]

The challenge is therefore generating anti-counterfeiting patterns that are difficult or impossible to replicate,[9] but yet can be produced rapidly and by a relatively simple technology. Methods such as lithography,[9c, 10] although offering spatial resolution down to few nanometres, are usually expensive and sequential in nature, *i.e.* multi-step and time consuming. Patterns of nanoparticles, especially with embedded gradients of shapes and sizes, are a good compromise between security, scalability and costs.[9d, 11] Nanoparticles of multiple shapes or sizes can be deposited within a given area, but this requires sacrificing substantial spatial resolution and involves sequential fabrication steps.

Here we show a single-step technology capable of printing at the "flick of switch" features made up of nanoparticles having multiple polyhedral shapes and sizes. The interparticle separation is completely adjustable, with gradients and patterns of resolution down to few

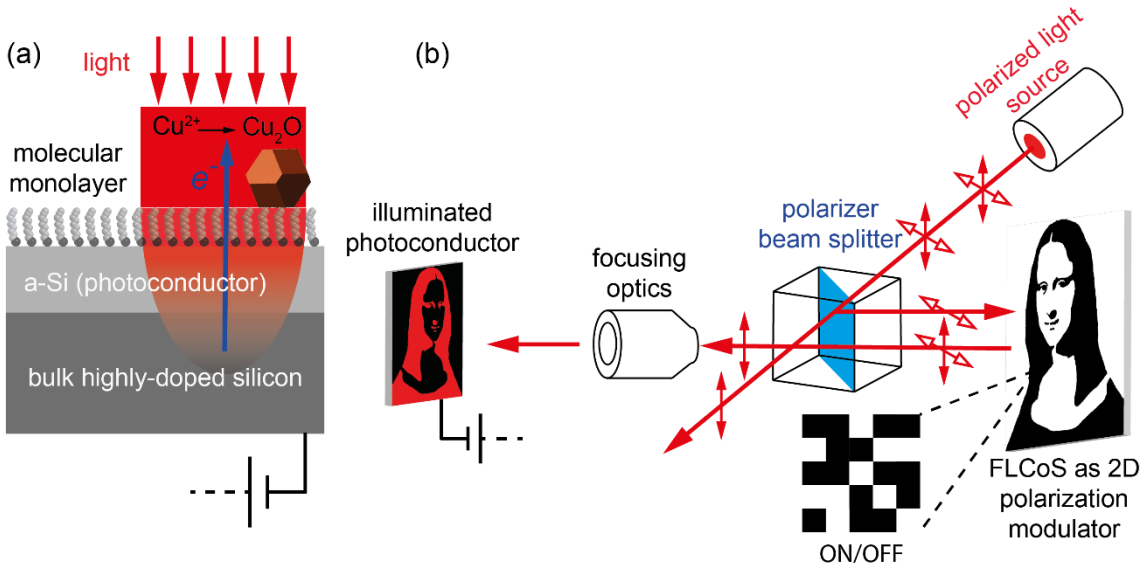

Figure 1. Photoelectrochemical assembly of nanocrystal arrays. (a) Cu^{2+} ions in an electrolyte solution are photoelectrochemically discharged to Cu^{+} and hydrolysed to form Cu_2O nanocrystals on the electrode surface. The deposition is confined in space and time to the illuminated regions of a photoconductor/electrolyte interface. The depiction of the interface, molecular monolayer and Cu_2O particles is not to scale. (b) A user-defined image, or a sequence of images, is projected on the interface with this light pattern being defined by the ON/OFF status of each pixel of a ferroelectric spatial light modulator (schematically depicted as black and white squares in figure). This large array of ON/OFF ferroelectric liquid crystals elements (over 3 million of FLCoS pixels in the space of about 2 cm^2) changes (or not, *i.e.* empty arrows heads) the 2D pattern of the light polarization that is reflected back towards the electrode via a polarizer beam splitter, hence it defines the image projected on the electrified photoconductor (a-Si).

micrometres being deposited within seconds. Key to this technology is modulation of electrode kinetics at amorphous silicon (a-Si henceforth) by visible light[12] (**Figure 1a**) and the use in electrochemistry of a spatial light modulator[13] designed for super resolution microscopy[14] (**Figure 1b**). The ink, *i.e.* the nanoparticles, is produced *in situ* by the photoelectrochemical reduction of Cu^{2+} ions to Cu_2O (Figure 1a).

Removal of an interfacial kinetic barrier at the semiconductor/electrolyte interface by means of supra-band gap illumination has been used previously for printing nanoparticles,[13, 15] DNA[16] and polymers,[17] but direct measurements of lateral growth of these patterns and the

possibility of two-dimensional (2D hereafter) light modulation towards parallel deposition of different polyhedral shapes and gradients of nanoparticles remains unexplored.

The structure of this article is as follows: i) we first explore the generation of Cu_2O nanoparticles at silicon photoelectrodes, with emphasis on defining the key variables in influencing the sharpness of surface patterns and provide insights on factors affecting the lateral growth of the patterns, ii) we investigate the scope and limits in using optics-only to tune local interparticle separation, iii) we define the relative weight of the bias and light variables in terms of guiding polyhedral shapes and sizes of the electrochemically-grown Cu_2O nanocrystals, and iv) we then apply these findings (i–iii) in the context of generating a pattern that encodes two sets of information: a 2D high resolution arrangement of nanocrystals with embedded hidden polyhedral signatures. Anti-counterfeiting validation by the end-user will only require examination of micrometre-scale patterns by a low-magnification and readily-avaialble optical microscope, while inspection of cryptic nanocrystal signatures by means of electron microscopy could be targeted in high-end applications.

2. Results and Discussion

In this work a light stimulus defines the "printing" area by means of locally removing the kinetic barrier for the discharge of metal ions at a photoconductor/electrolyte interface. A user-defined image, or sequence of images, is projected on the interface with the light pattern being defined by the ON/OFF status of each one of the over 3 million pixels of a ferroelectric spatial light modulator (FLCoS in Figure 1b). Our initial step was therefore to measure the correlation between the light stimulus hitting the photoconductor surface and the nanoparticle pattern. In other words, to measure experimentally how the cumulative effect of factors such as light intensity, light collimation, phase modulation by the FLCoS, focus, light penetration

and charge diffusion in the photoconductor affects the conversion of a given bitmap image file into a geometric pattern of metal oxide particles.

We started by exploring the effects of light intensity, wavelengths and photoconductor thickness in the discharge of Cu^{2+} ions by creating a conducting channel through the a-Si layer. For the Cu^{2+} reduction to happen at a measurable rate, *i.e*. for patterns to form within a timescale of seconds to minutes, enough photogenerated charge carriers must reach the highly-doped bulk silicon substrate (see Figure 1a), meaning an appropriate combination of light wavelength, photoconductor thickness and light intensity. The light penetration depth (*x*, the distance into the material at which the light intensity drops to *ca*. 37%) is a function of the wavelength of the light (λ) and the extinction coefficient (*k*) ($x = \frac{\lambda}{4\pi k}$). By using a red light (λ = 625 nm) we found that an a-Si layer of thickness of about 1 μm allows for Cu^{2+} discharge, and formation of Cu_2O nanoparticles arrays, already at a very low light intensity (*ca*. 100 lx, Figure S1 and S2, Supporting Information), while a thicker layer of 4 μm requires substantially higher intensities or deposiotion times of several minutes. This aspect, *i.e.* even a dim light suffices to trigger the onset of metal oxide deposition, becomes extremely important when changes of light intensity are systematically explored in the context of tuning densities and shapes (*vide infra*).

We then proceeded to evaluate to what extent the image projected at the reaction site, *i.e.*, the electrode surface, is a match of the bitmap image file that is being used to generate it. Light scattering and non-ideal collimation/focusing cannot be completely eliminated and therefore there is the possibility of a departure between image file and image projected at the electrified interface (Figure S3, Supporting Information). The FLCoS is an array of 2048 × 1536 polarization-modulation elements, each 8.3 × 8.3 μm in size, and the rest of the optic system defines the size of a pixel once projected on the substrate. In the absence of electrolyte and of the FTO counter electrode each pixel at the silicon surface is appearing as a perfect square of

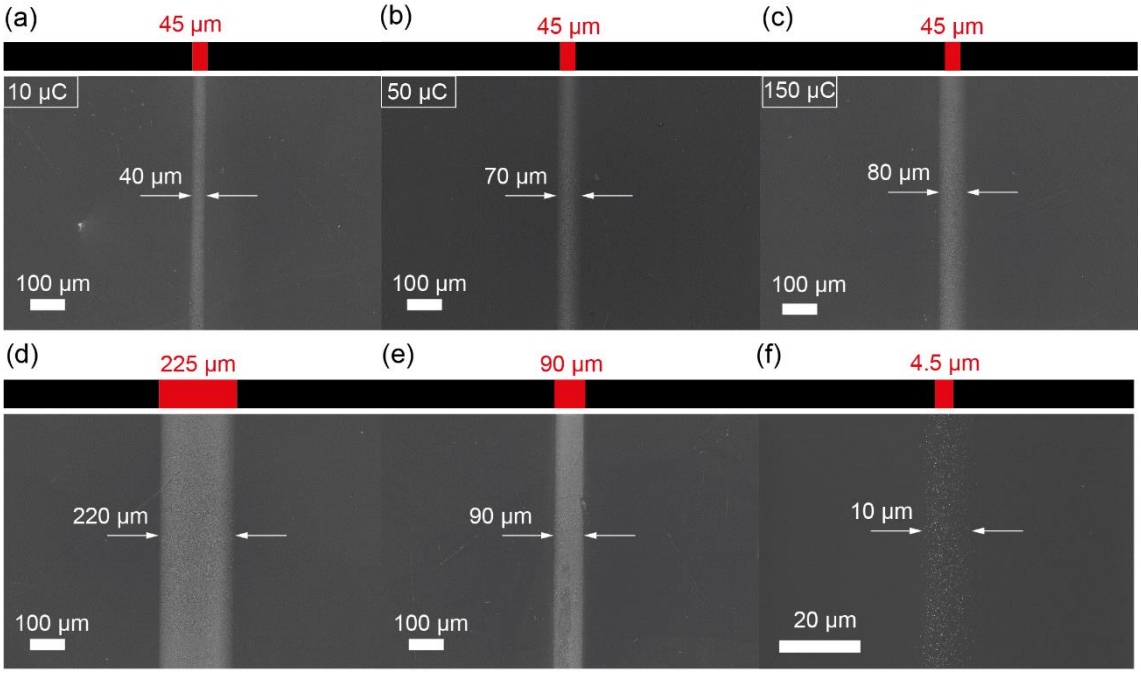

Figure 2. Micropattern sharpness as a function of illumination characteristics and amount of charge transferred. SEM images for Cu_2O "lines" that are deposited on the a-Si film by illuminating only a discrete area of the photoelectrode. The width of the illuminated area is shown in red ink on the top of each micrograph, and the actual width of the electrodeposited "line" is specified with white ink labels on the centre of each image. Panels (a–c) show the relationship between the sharpness of the Cu_2O feature and the total charge transferred during the Cu^{2+} discharge. Panels (d–f) illustrate the lower achievable limit of the feature size. (f) The smallest features are obtained by limiting amount of charge being transferred and by illuminating a single-pixel width line, giving a resolution of *ca*. 10 µm for this system. The electrolytic solution was 50 mM of $CuSO_4$ and 0.5 M of K_2SO_4. For (d–f) the total charge transferred per unit of illuminated area was kept constant (1 µC/µm^2). The electrodeposition potential was stepped from the open circuit potential to –0.5 V.

4.5 × 4.5 µm, in principle allowing to project features as big as *ca*. 60 mm^2 or as little as *ca*. 20 µm^2. However, for the actual nanoparticle printing, the lateral diffusion of photogenerated electrical carriers towards dark areas of the silicon surface is expected to be a key factor.[18] Data in **Figure 2a–c** shows that the sharpness of the Cu_2O feature can be limited by controlling the amount of charge transferred during its electrodeposition. Further, by narrowing the light profile to its minimum value of a single-pixel width (**Figure 2d–f**), and by controlling the charge being transferred (Figure S4, Supporting Information) a feature as small as small as 10 µm can be deposited (Figure 2f).

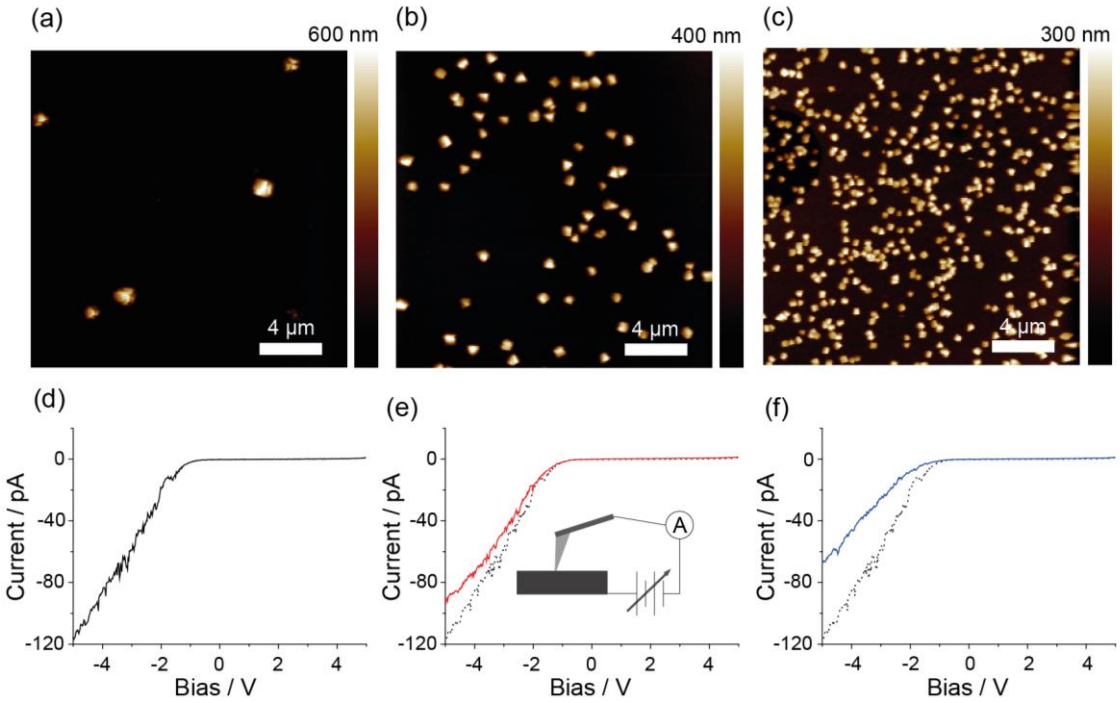

Figure 3. Changes to the local substrate conductivity *vs* Cu_2O surface coverage. (a–c) AFM height images for samples of progressively larger fractional surface coverage of Cu_2O (1%, 7% and 26% respectively). (d–f) Representative current–potential curves (I–Vs) acquired on the a-Si substrate. The dotted line in panels (e) and (f) is the I–V shown in (d) and it is intended for comparison purposes only. I–Vs are sampled using a platinum AFM tip at a constant force of 2.25 µN. The bias routing is from the silicon substrate to the platinum AFM tip. The particles from panels (a–c) are electrodeposited within a single a-Si substrate by projecting a progressively increasing fraction of ON pixels (Figure S6, Supporting Information, 0.2, 0.3 and 0.4, respectively) and stepping the potential from the open circuit to $E = -0.1$ V until a charge of 9 mC has passed.

The mismatch between the printed pattern and the light profile, *i.e.* the degree of the particles' lateral growth off the illuminated areas, increases as the feature is narrowed (Figure 2d–f) but reaches saturation as the transferred charge increases, *i.e.* at high Cu_2O coverage (*e.g.* Figure 2a–c, and Figure S4, Supporting Information). The latter is presumably because copper traces are known to reduce the lifetime of charge carriers in silicon[19] and/or because the large coverage of Cu_2O may be reducing the efficiency of electrons ejection off from the a-Si (*i.e.* reducing electrochemical currents), preventing the growth of new particles near the high-density areas (*e.g.* the feature's edges). To gain insights on this aspect we have used conductive atomic force microscopy (AFM) to map electrically and with high spatial

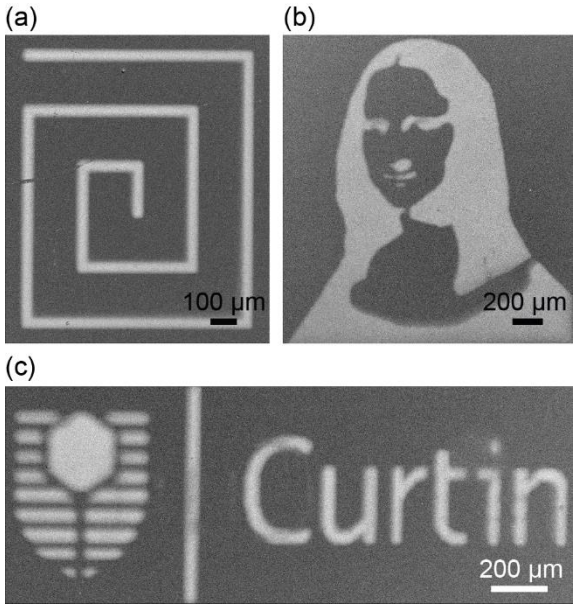

Figure 4. SEM images of Cu_2O nanoparticle patterns. The patterns recreate a user-defined bit-map file loaded into the FLCoS microprojector and are electrochemically printed in a parallel fast process within seconds (*ca*. 20 seconds). The patterns were electrodeposited by stepping the potential from the open circuit to –0.5 V until reaching a total charge of 100 µC (a, c) or 200 µC (b) while projecting an image of the corresponding pattern at a constant illumination (1030 lx). Bmp files used to generate these patterns are shown in Figure S5.

resolution the a-Si surface as a function of the local fractional surface coverages of Cu_2O particles (**Figure 3a–c**). AFM current–potential curves sampled on the silicon surface show a progressive decrease in the forward current as the Cu_2O surface coverage increases (**Figure 3d–f**), indicating a less efficient electron ejection from the a-Si, therefore probably making it progressively more difficult for particles to grow after a certain amount of Cu_2O has already been deposited (*e.g*. 26% in Figure 3). This aspect may account in part to the increased sharpness of the features as the amount charge transferred is increased (Figure 2a–c).

This printing method can draw arbitrary and high-resolution patterns in few seconds, and using only clean stimuli of light and potential (**Figure 4**). However, the high resolution and evading the needs of masking or templating, is in itself by no means technologically or conceptually unique, with high-quality inkjet printers[20] being readily available. Unique advantages of our FLCoS/photoelectrochemcial platform are that it is parallel, single-step,

low-cost and does not require pre-synthesized nanoparticles. Additionally, we reasoned that this platform may make it possible of depositing polyhedral signatures at a location defined at will by the experimentalist. We started exploring this possibility by studying the influence of parameters affecting the photoelectrochemical discharge of Cu^{2+} in terms of the morphology, size and density in the deposited Cu_2O nanoparticles.

The density of particles deposited by discharging ions in solution depends on the number of nucleation sites per area.[21] Hence, the nanoparticle density is expected to relate to the local density of ON pixels (average number of ON pixels per unit area). As shown in **Figure 5a** this aspect controls the nanoparticle density in a pattern with progressively decreasing densities along the *x*-direction along a sample. The projected image consists of a pattern having increasing density of ON pixels along the *x*-direction (Figure S6, Supporting Information), which in turn generates progressively more nucleation sites moving along this direction. What is also evident in Figure 5a is a link between the nanoparticle's spacing and their shapes. We then proceeded to investigate the origin of this link in order to achieve means to independently address densities, sizes and shapes within the scale of these structures. The size and the density of particles can be controlled by a careful selection of light intensity, charge density and applied potential. For instance, in **Figure 5b** (and Figure S7, Supporting Information) the size and density were controlled independently by setting a constant ON pixel density and illuminating sequentially areas along the *x*-direction with increasing the amount of charge transferred. The other systematic change that becomes apparent in moving along the *x*-direction in Figure 5a (the direction of increasing densities of ON pixels) is a drop in the particles "cubicity" for the more intense illuminations. Cubicity is here defined as the ratio of ‹100› facets area over the total nanoparticle surface area (**Figure 6a**). The following section expands on this aspect as this is the basis for an additional level of uniqueness to these patterns; a specific polyhedral shape can be confined to a selected

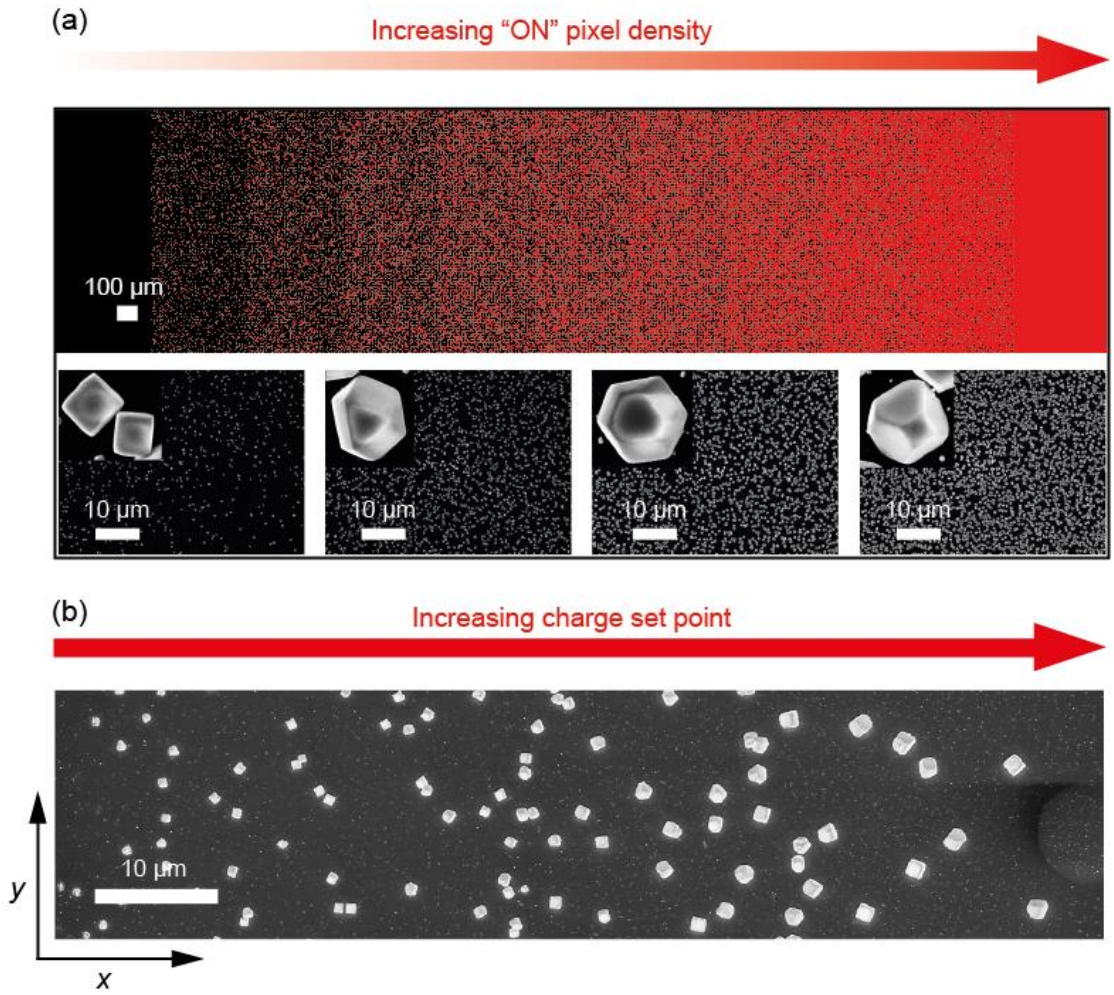

Figure 5. Nanoparticle arrays with localized changes to particle densities and sizes. (a) The local spacing between Cu_2O nanoparticles is fine-tuned by adjusting the number of ON pixels projected on a certain area of the photoconductor (a, top). This enables building arrays of defined interparticle distances across a single macroscopic substrate in a parallel process. The local density of ON pixels (defined as the ratio of ON pixels over the total number of pixels) is increased along the *x*-direction from 0 to 1 in steps of 0.1 every 100 pixels (a, top). (a, bottom) SEM images taken along the *x*-direction on a Cu_2O pattern generated by projecting the top (a) panel image. From left to right the density of ON pixels are 0.2, 0.3, 0.5 and 0.9, resulting in a Cu_2O particles surface coverage of approximately 7%, 20%, 30% and 45%, respectively. The electrodeposition parameters are: E = 0.0 V, light intensity at the electrode surface for the 100% ON pixel level is 1030 lx and 9 mC of charge are passed. (b) SEM image of a Cu_2O pattern that is generated by increasing the transferred charge density on sequentially illuminated areas along the *x*-direction (from 10 µC to 500 µC). The particles were electrodeposited at E = –0.1 V under 390 lx in the presence of 3 mM of KCl.

area, which is only known to the experimentalist, and most importantly, this cryptic crystal signature can be set independently to any pattern of size and density. Some of the factors affecting shapes of Cu_2O nanocrystals can be found elsewhere,[15c] where the electrical

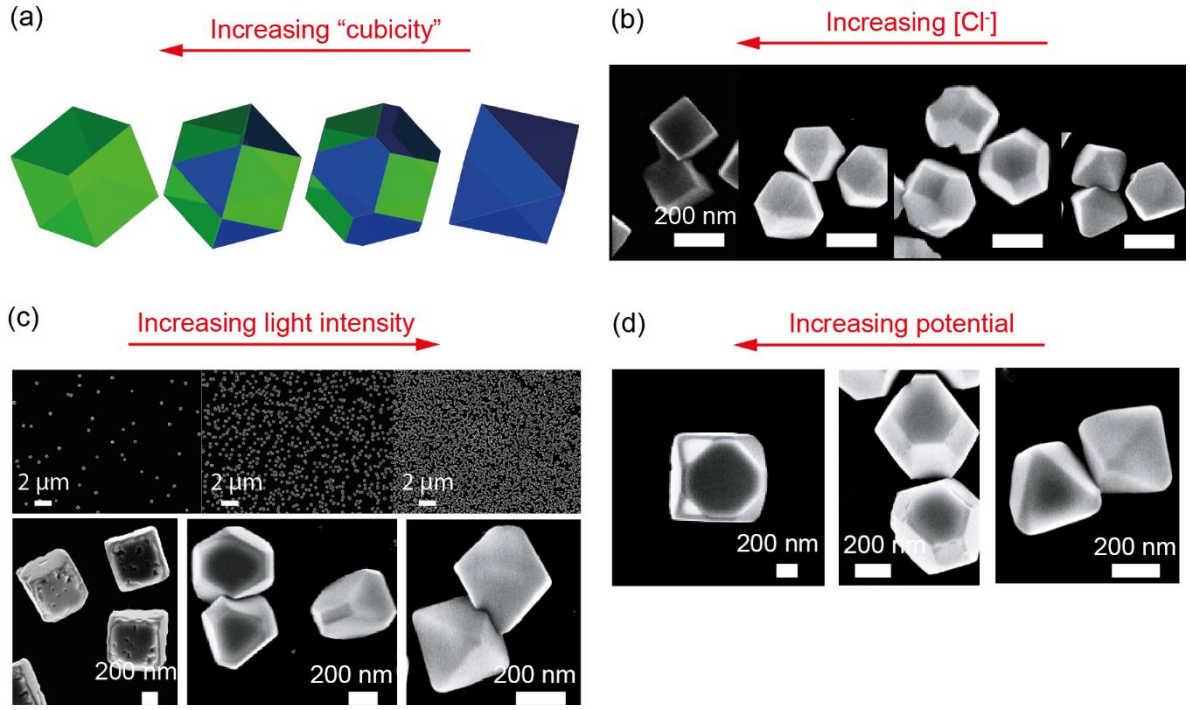

Figure 6. SEM images of Cu_2O nanoparticles and its progressively transition from cubic to octahedral shapes (a) upon changes to either (b) bulk chloride concentrations (from left to right, the chloride concentration is decreased from 0.3 mM, 0.1 mM, 0.03 mM to <0.015 mM, with the deposition potential being set 0.0 V and the light intensity to 1030 lx), or (c) light intensity (from left to right the intensity increases from 170 lx, 390 lx to 1030 lx, with the deposition potential being 0.0 V and the chloride concentration <0.015 mM, or (d) deposition potential (from left to right, the deposition potential is 0.1 V, 0.0 V and –0.1 V, with the chloride concentration being <0.015 mM and a light intensity of 1030 lx).

properties of Cu_2O particles was reported in the context of developing single-particle electrical circuits, expanding seminal work on facet-dependent electrical conductivity.[22] As mentioned above,[15c] it is evident that the Cu_2O nanocrystals in Figure 5a (insets) all have a different shape, which appears to be linked to the nanoparticle density changed by changing the ON pixel density of the FLCoS projector. This is suggestive as it points to a link between particle density and anisotropic growth of the crystals. Changes to the bulk concentration of a bulk additive that is known to adsorb on a specific crystallographic face is an established method to control the polyhedral shape of a nanoparticle. For Cu_2O nanocubes, for instance, they are obtained when adding chloride that adsorbs preferentially on the ‹100› face,[23] with a progressive transition to octahedral particles (Figure 6a) as the chloride concentration

decreases (**Figure 6b**), resembling the trend observed when decreasing the nanoparticle density (Figure 5a). It is generally accepted that cubes results from the faster growth rate in the ‹111› direction,[24] and in 2011 theoretical paper, Suleiman *et al.* predicted a progressive transition from octahedral (with only ‹111› planes) to cubic (with only ‹100› planes) particle shapes of Cu crystals as a function of the chlorine chemical potential.[25] This can be understood in terms of the surface free energy of the ‹100› and ‹111› planes calculated as a function of the chlorine chemical potential, which depends on the bulk chlorine concentration. This explains the trend in Figure 6b, showing a progressive transition from octahedral to cubic particles as the bulk chloride concentration increases. A similar effect was recently reported in the context of tuning particle shapes to study current rectification in Cu_2O nanocrystals/silicon junctions.[15c] A complete understanding of the factors at play aspect will require substantially more work, but circunstantial evidence suggests the existence of a link between chloride adsorption and the observed trend in shapes. Changes in nanoparticle densities, as for the data shown in Figure 5a and 6c, are such that we can reasonably assume that the Cl^--to-Cu_2O surface ratio is progressively increased in moving from right to left panels. Analogously, the nanocrystal shape appears to depend on the electrochemical potential of chloride ($\overline{\mu}_{Cl}$, Figure 6d) as it reasonable to assume that the electrochemical potential of a charged ion is a function of the surface potential ($\overline{\mu}_{Cl} = \mu_{Cl} + zF\Phi$).

A literature search points out that control on the shape of particles by means of potential has been only explored at a limited extent, with only few experimental observations.[15c, 26] In 2013 Bonnet and Marzari theoretically predicted changes in the equilibrium shape of nanocrystals could be driven by changes to the anisotropic adsorption of ions in response to changes to an applied bias.[27] By changes in the applied potential the chemical potential can be adjusted and hence the surface energy of the crystal. It would be then possible to make

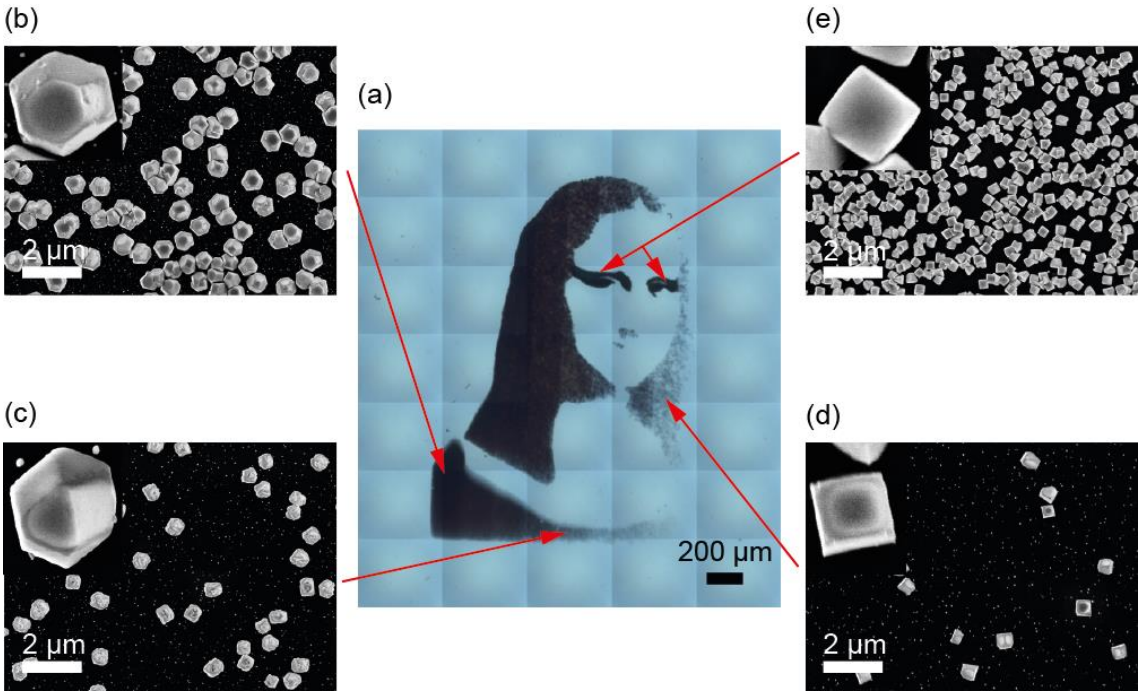

Figure 7. Hiding of a cryptic polyhedral signature. Gradients of shapes and densities embedded in a "Mona Lisa". (a) Optical microscopy image of the "Mona Lisa" pattern. (b–e) SEM images showing the evolution of the Cu_2O shapes within the patterned area. Electrodeposition was done at –0.1 V at a constant illumination by projecting a sequence of two images: i) a Mona Lisa without eyes and with a gradient of ON pixels density along the *x*-direction (left to right, Figure S8a, Supporting Information) in a solution containing <15 µM of Cl^- (panels b–d) until reaching a total charge of 2.2 µC, and ii) the Mona Lisa eyes (Figure S8b, Supporting Information) deposited from a solution containing 3 mM Cl^- by passing 1.6 µC (e).

changes to the (electro)chemical potential by bias changes to adjust the surface energy and hence tune the particle shape. When the concentration of bulk chloride ions is fixed, bias-driven changes to the chemical potential of halide explains why it is possible to predictably guide the octahedron-to-cube transition by a simple change to the external bias. Notably, hydrogen adsorbs favorably on the platinum ‹100› face and it is possible that bias-dependent anisotropic adsorption of hydrogen is a significant factor accounting for the high "cubicity" observed for platinum particles that forms when hydrogen diffuses across fuel cells membranes towards the cathode.[28] We remark, however, that our experimental evidence, although supported by theoretical modelling and similar observations in other materials,

remains at present indirect and that a conclusive explanation will require a direct spectroscopic evidence of chloride adsorbing preferentially on the Cu_2O ‹100› face.

In summary, the ability to define the nanoparticle printing area by means of localizing charge transfer events in 2D can be achieved with high spatial resolution (Figures 1–3). Both these aspects can also be coupled to a control of nanoparticle sizes (Figure 5b), spacing between neighbors (Figure 5a) and control on the polyhedral shape of the crystal (Figure 6), hence allowing for the construction of complex patterns with a scope as anti-counterfeiting printing technology.[29] **Figure 7** is such an example, highlighting the multiple levels of security that can be embedded in a small pattern using this platform. Figure 7 is an array of Cu_2O particles in the shape of well-known portrait. Not visible to the eye of the observer, but only becoming apparent after SEM analysis, the stylized Mona Lisa conceals an user-defined gradient of Cu_2O particle densities that overlaps with a gradient of polyhedral shapes along the *x*-direction. An additional cryptic feature is then deliberately added, and it is in the form of a region of high "cubicity" in the Mona Lisa's eyes. This last feature is at odds with the regular polyhedral changes across the sample and its exact location is only known to the person that prepared the pattern.

3. Conclusion

In conclusion, we have developed a printing technology that is non-contact, fast, low cost and scalable by using simple local assembly rules (voltages and local density of bright pixels). Arrays are formed within seconds without the need of physical masks or chemical templating. A custom adaptation of a commercial spatial light modulator is used to generate a high-resolution light pattern on a photoconductor and copper ions are discharged to form arrays of Cu_2O nanocrystals. Electrochemically printed features of Cu_2O are an exact match of the projected image as long as the pattern lateral growth outside the illuminated areas is prevented by controlling the amount of charge transferred. The electron ejection from the

substrate, studied by high resolution electrical mapping in AFM, is less favorable at high surface coverages of Cu_2O, enebling to print sharper patterns. The interparticle distances within the array and the degree of "cubicity" of the nanocrystals can be systematically adjusted by manipulating the local density of ON (bright) pixels in the projected image. By adding small amounts of chloride we show that it is also possible to attain independent control of the interparticle distance or shapes. The nanocrystal shape was also found to be linked to the electrodeposition potential in a predictable and adjustable manner. We emphasise that the control over space of the nanocrystal shape, size and interparticle distance is accomplished without the use of organic capping agents, additives, grafted chemical gradients or templates.

4. Experimental Section

Materials. Unless stated otherwise all chemical were of analytical grade and used as received. Sulfuric acid (Sigma-Aldrich, Puranal^{TM}, 95-97%), ammonium fluoride (Sigma-Aldrich, Puranal^{TM}, 40%,), 1,8-nonadiyne (Sigma-Aldrich, 98%), ammonium sulphite (Sigma-Aldrich, 92%) were used in wafer cleaning, etching and hydrosilylation procedures.[12-13, 27] Copper sulphate (Chem-Supply, 99.5%), potassium sulphate (Ajax Finichem, 99%), and potassium chloride (Ajax Finichem, 99.8%) were used to prepare the electrolytic solutions. Redistilled solvents were used for the surface modification procedures. Milli-Q^{TM} water with a resistivity >18.2 MΩ cm was used.

Preparation and chemical functionalization of the amorphous silicon film. Si(100) wafers with a resistivity of 0.001−0.004 Ω cm (Siltronix, S.A.S, Archamps, France) were rinsed with DCM, dried under a stream of argon, and immersed in piranha solution (a 3:1, v/v, mixture of concentrated sulfuric acid and 30% hydrogen peroxide) for 10 min. Samples were then rinsed with water before being etched for 60 s in an aqueous solution of hydrofluoric acid (48%

HF/water, 1:10, v/v) kept at 30 ºC. The hydrogen-terminated wafers were then copiously rinsed with water. A film of amorphous silicon (a-Si) with a resistivity of approximately 10^4 Ω·cm was then deposited on the hydrogen-terminated wafers using an Oxford Instruments Plasmalab 100 plasma-enhanced chemical vapour deposition system. SiH_4 gas was used as the a-Si precursor and argon gas was employed as the carrier. Plasma was generated using a 13.56 MHz 300W RF generator with auto matching unit. Deposition of the a-Si film was performed at 300 ºC and under a pressure of 5×10^{-2} mTorr with the deposition time being varied according to the calibration curve of the equipment. The a-Si thickness was confirmed *ex situ* by SEM cross-section analysis. Chemical derivatization of the a-Si film by hydrosilylation of a 1,8-nonadiyne liquid sample followed a previously reported procedure.[12] In brief, the a-Si coated silicon wafers were cut into 1 × 1 cm pieces, cleaned with DCM and water, immersed in piranha solution (100 °C, 20 min), rinsed thoroughly with water, etched for 10 min in 40% aqueous ammonium fluoride solution (degassed by bubbling with argon gas for 20 min and added a small amount of ammonium sulphite), rinsed sequentially with water and DCM, dried under a nitrogen stream and placed on a glass sheet before dropping *ca*. 50 µl of 1,8-nonadiyne on the a-Si surface. To limit evaporation, the sample was top-contacted with a quartz slide. The samples were kept under positive nitrogen pressure and rested under UV light for 2 h (Vilber, model VL-215.M, λ = 312 nm, nominal power output of 30 W and positioned approx. 200 mm away from the silicon sample). Samples were then rinsed several times with DCM, rested for 12 h in a sealed vial under DCM at +4°C and blown dry under nitrogen before analysis or further modification.

Electrochemical deposition of Cu_2O nanocrystals. Electrochemical experiments were performed in a three-electrode electrochemical cell (Figure S3, Supporting Information) using an Ag/AgCl (sat. KCl) reference electrode, an FTO slide as the counter electrode (FTO on a 1.1 mm thick glass slide, 8 Ω sq^{-1}, Solaronix SA, Switzerland) and the monolayer-modified a-

Si/silicon wafer as the working electrode. The electrochemical parameters were applied and recorded with a commercial potentiostat (650D, CH Instruments). The Cu_2O nanoparticles were electrodeposited from a solution containing 50 mM $CuSO_4$, 0.5 M of K_2SO_4 and the specified amount of KCl. The working electrode was illuminated through the FTO electrode and electrolyte using a projection system described in details elsewhere,[13] based on a ferroelectric liquid crystal on silicon (FLCoS) spatial light modulator (model QXGA-3DM from Forth Dimension Displays Ltd). The projected images were uploaded as bitmap files to the printed circuit board memory of the microdisplay. Bitmap files were generated using MATLAB® and Adobe Photoshop softwares. The images at different ON pixel density were generated by a defined total number of ON pixels of a certain area by a pseudorandom location of the ON pixels in the image. The FLCoS operates in amplitude modulation and each ON pixel has a similar function to a combination of a mirror and quarter-wave plate.[30] The pixel density of a specific area is defined as the number of ON pixels divided by the total number of pixels in that area. The system allows to modulate the intensity of the projected light by changing the LED forward current.

Sample imaging and electrical characterization. The scanning electron microscopy (SEM) images were obtained using a Zeiss Neon 40EsB FESEM equipped with a Schottky field emission gun operating at 5 kV and a chamber pressure of approximately 4×10^{-6} mbar and a Tescan Mira3 FESEM, also equipped with a Schottky field emission gun operating at 5 kV, and a chamber pressure of approximately 3×10^{-2} Pa. Atomic force microscopy (AFM) experiments were performed with a Bruker Dimension Icon atomic force microscope using conductive platinum tips (Rocky Mountain Nanotechnology AFM probes, 25Pt300B, with spring constant of 18 N m^{-1}). The images were acquired at a resolution of 512 × 512 points. Current–potential data were taken at a constant force of 2.25 μN, a voltage sweep rate of 1 V/s and setting the current gain to 20 pA/V. The AFM tip is grounded and the bias is applied from

the substrate to the tip. We used the sign convention of potential and current being of a positive sign when the substrate is biased positive with respect to the AFM tip. Optical images were acquired with the optical microscope incorporated in a Nicolet iN10 MX infrared microscope by acquiring consecutives images to fully cover the area of interest.

Supporting Information
Supporting Information is available from the Wiley Online Library or from the author.

Acknowledgements
This work was supported by grants from the Australian Research Council (DE160100732 (S.C.), DE160101101 (N.D.) and DP150103065 (J.J.G. and S.C.)). The authors acknowledge the use of Curtin University's Microscopy & Microanalysis Facility, whose instrumentation has been partially funded by the University, State and Commonwealth.

Received: ((will be filled in by the editorial staff))
Revised: ((will be filled in by the editorial staff))
Published online: ((will be filled in by the editorial staff))

References

[1] P. Chaudhry, A. Zimmerman, in *Protecting Your Intellectual Property Rights: Understanding the Role of Management, Governments, Consumers and Pirates*, Springer New York, New York, NY 2013, 7.
[2] https://iccwbo.org/global-issues-trends/bascap-counterfeiting-piracy/.
[3] http://www.safetraces.com/.
[4] R. N. Harding, C. A. Hara, S. B. Hall, E. A. Vitalis, C. B. Thomas, A. D. Jones, J. A. Day, V. R. Tur-Rojas, T. Jorgensen, E. Herchert, R. Yoder, E. K. Wheeler, G. R. Farquar, *Aerosol Sci. Technol.* **2016**, *50*, 429.
[5] J. Wang, C. F. Wang, S. Chen, *Angew. Chem., Int. Ed.* **2012**, *124*, 9431.
[6] a) R. Xuan, J. Ge, *Langmuir* **2011**, *27*, 5694; b) P. Kumar, K. Nagpal, B. K. Gupta, *ACS Appl. Mater. Interfaces* **2017**, *9*, 14301.
[7] H. Nam, K. Song, D. Ha, T. Kim, *Sci. Rep.* **2016**, *6*, 30885.
[8] a) L. Meraviglia, *Business Horizons* **2018**; b) B. Yoon, J. Lee, I. S. Park, S. Jeon, J. Lee, J.-M. Kim, *J. Mater. Chem. C* **2013**, *1*, 2388.
[9] a) K. Jiang, L. Zhang, J. Lu, C. Xu, C. Cai, H. Lin, *Angew. Chem., Int. Ed.* **2016**, *55*, 7231; b) T. Sun, B. Xu, B. Chen, X. Chen, M. Li, P. Shi, F. Wang, *Nanoscale* **2017**, *9*, 2701; c) Y. Cui, R. S. Hegde, I. Y. Phang, H. K. Lee, X. Y. Ling, *Nanoscale* **2014**, *6*, 282; d) M. You, J. Zhong, Y. Hong, Z. Duan, M. Lin, F. Xu, *Nanoscale* **2015**, *7*, 4423; e) V. J. Cadarso, S. Chosson, K. Sidler, R. D. Hersch, J. Brugger, *Light: Sci. Appl.* **2013**, *2*, e86; f) H. J. Bae, S. Bae, C. Park, S. Han, J. Kim, L. N. Kim, K. Kim, S. H. Song, W. Park, S. Kwon, *Adv. Mater.* **2015**, *27*, 2083.
[10] a) S. Han, H. J. Bae, J. Kim, S. Shin, S. E. Choi, S. H. Lee, S. Kwon, W. Park, *Adv. Mater.* **2012**, *24*, 5924; b) L. Qin, M. J. Banholzer, J. E. Millstone, C. A. Mirkin, *Nano Lett.* **2007**, *7*, 3849.

[11] a) B. Creran, B. Yan, D. F. Moyano, M. M. Gilbert, R. W. Vachet, V. M. Rotello, *Chem. Commun.* **2012**, *48*, 4543; b) B. Duong, H. Liu, L. Ma, M. Su, *Sci. Rep.* **2014**, *4*, 5170.
[12] Y. B. Vogel, L. Zhang, N. Darwish, V. R. Gonçales, A. Le Brun, J. J. Gooding, A. Molina, G. G. Wallace, M. L. Coote, J. Gonzalez, S. Ciampi, *Nat.. Commun.* **2017**, *8*, 2066.
[13] Y. B. Vogel, V. R. Gonçales, J. J. Gooding, S. Ciampi, *J. Electrochem. Soc.* **2018**, *165*, H3085.
[14] B.-C. Chen, W. R. Legant, K. Wang, L. Shao, D. E. Milkie, M. W. Davidson, C. Janetopoulos, X. S. Wu, J. A. Hammer, Z. Liu, B. P. English, Y. Mimori-Kiyosue, D. P. Romero, A. T. Ritter, J. Lippincott-Schwartz, L. Fritz-Laylin, R. D. Mullins, D. M. Mitchell, J. N. Bembenek, A.-C. Reymann, R. Böhme, S. W. Grill, J. T. Wang, G. Seydoux, U. S. Tulu, D. P. Kiehart, E. Betzig, *Science* **2014**, *346*.
[15] a) N. Liu, F. Wang, L. Liu, H. Yu, S. Xie, J. Wang, Y. Wang, G.-B. Lee, W. J. Li, *Sci. Rep.* **2016**, *6*, 32106; b) S. Y. Lim, Y.-R. Kim, K. Ha, J.-K. Lee, J. G. Lee, W. Jang, J.-Y. Lee, J. H. Bae, T. D. Chung, *Energy Environ. Sci.* **2015**, *8*, 3654; c) Y. B. Vogel, J. Zhang, N. Darwish, S. Ciampi, *ACS Nano* **2018**, *12*, 8071.
[16] B. Y. Chow, C. J. Emig, J. M. Jacobson, *Proc. Nat. Acad. Sci. U. S. A.* **2009**, *106*, 15219.
[17] a) S.-H. Huang, L.-S. Wei, H.-T. Chu, Y.-L. Jiang, *Sensors* **2013**, *13*, 10711; b) M. H. Choudhury, S. Ciampi, Y. Yang, R. Tavallaie, Y. Zhu, L. Zarei, V. R. Goncales, J. J. Gooding, *Chem. Sci.* **2015**, *6*, 6769; c) Y. Liu, C. Wu, H. S. S. Lai, Y. T. Liu, W. J. Li, Y. J. Shen, *Micromachines* **2017**, *8*, 192.
[18] W. Moritz, T. Yoshinobu, F. Finger, S. Krause, M. Martin-Fernandez, M. J. Schöning, *Sens. Actuators, B* **2004**, *103*, 436.
[19] H. Väinölä, E. Saarnilehto, M. Yli-Koski, A. Haarahiltunen, J. Sinkkonen, G. Berenyi, T. Pavelka, *Appl. Phys. Lett.* **2005**, *87*, 032109.
[20] C. W. Sele, T. von Werne, R. H. Friend, H. Sirringhaus, *Adv. Mater.* **2005**, *17*, 997.
[21] G. Gunawardena, G. Hills, I. Montenegro, B. Scharifker, *J. Electroanal. Chem. Interf. Electrochem.* **1982**, *138*, 225.
[22] a) C.-S. Tan, S.-C. Hsu, W.-H. Ke, L.-J. Chen, M. H. Huang, *Nano Lett.* **2015**, *15*, 2155; b) C.-S. Tan, Y.-J. Chen, C.-F. Hsia, M. H. Huang, *Chem. Asian J.* **2017**, *12*, 293; c) C.-H. Kuo, Y.-C. Yang, S. Gwo, M. H. Huang, *J. Am. Chem. Soc.* **2011**, *133*, 1052; d) C.-S. Tan, P.-L. Hsieh, L.-J. Chen, M. H. Huang, *Angew. Chem. Int. Ed.* **2017**, *56*, 15339.
[23] K.-S. Choi, *Dalton Trans.* **2008**, 5432.
[24] D. Wang, M. Mo, D. Yu, L. Xu, F. Li, Y. Qian, *Cryst. Growth Des.* **2003**, *3*, 717.
[25] I. A. Suleiman, M. W. Radny, M. J. Gladys, P. V. Smith, J. C. Mackie, E. M. Kennedy, B. Z. Dlugogorski, *J. Phys. Chem. C* **2011**, *115*, 13412.
[26] a) D. Zhang, P. Diao, Q. Zhang, *J. Phys. Chem. C* **2009**, *113*, 15796; b) M. Subhramannia, K. Ramaiyan, V. K. Pillai, *Langmuir* **2008**, *24*, 3576; c) B. J. Murray, Q. Li, J. T. Newberg, E. J. Menke, J. C. Hemminger, R. M. Penner, *Nano Lett.* **2005**, *5*, 2319.
[27] N. Bonnet, N. Marzari, *Phys. Rev. Lett.* **2013**, *110*, 086104.
[28] P. J. Ferreira, Y. Shao-Horn, *Electrochem. Solid-State Lett.* **2007**, *10*, B60.
[29] Patterns are stable under ambient conditions and are resistant to mechanical stress. For instance, the adhesion of the Cu2O particles cannot be competed out and attempts to "peel off" the patterns from the a-Si substrate using either strong adhesive tapes were not successful (Figure S9, Supporting Information). Furthermore, the polyhedral characteristics of the particles are also stable in air over the time scale of weeks (Figure S10, Supporting Information).
[30] http://www.forthdd.com/technology/amplitude-modulation/.

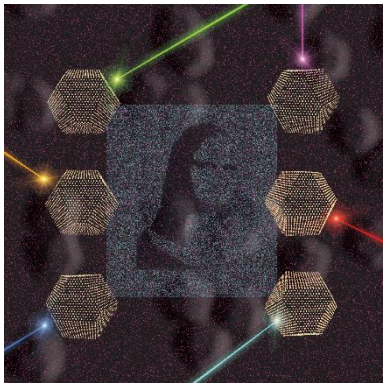

Cryptic nano-inks. Development of a photo-electrochemical printing technology with applications in the assembly of nanoparticles-based electrical circuitry or anti-counterfeiting labels. This technology is based on a parallel modulation of both the electrode kinetics at the silicon/electrolyte interface as well as the light-assisted control of adsorption of halide ions on growing metal oxide particles.